JOURNAL OF GEOPHYSICAL RESEARCH, VOL. 103, NO. E7, PAGES 16,841–16,853, JULY 25, 1998

Tectonic evolution of Bell Regio, Venus: Regional stress, lithospheric flexure, and edifice stresses

Patricia G. Rogers[1]

RAND, Washington, D. C.

Maria T. Zuber

Department of Earth, Atmospheric, and Planetary Sciences, Massachusetts Institute of Technology, Cambridge

Abstract. In order to understand the relationship between volcanic and tectonic processes and the stress state in the lithosphere of Venus, we analyzed the stress environments and resulting tectonic features associated with the major volcanic edifices in Bell Regio, using Magellan synthetic aperture radar (SAR) images and altimeter measurements of topography. The major volcanoes of Bell Regio, Tepev Mons and Nyx Mons, exhibit tectonic characteristics that are unique relative to other volcanic edifices on Venus. The most prominent distinction is the lack of large rift zones within the overall highland uplift, which characterize many other highland rises on Venus. Also, previous studies have determined that many large Venus volcanoes exhibit radial tectonic structures on their flanks but generally lack the circumferential graben which surround volcanoes on Earth and Mars. Tepev and Nyx Montes exhibit both the radial tectonic features associated with other Venusian edifices and numerous concentric graben. Nyx Mons implies a more distributed magmatic system by its broad shape, radial chains of pit craters, and expansive flow fields, whereas Tepev Mons is a more centralized volcanic system, with limited associated long flows. We investigate the regional stresses associated with Bell Regio and structural features believed to be a consequence of lithospheric flexure due to volcanic loading, modeling both Nyx Mons and Tepev Mons as axisymmetric loads with Gaussian mass distributions on an elastic plate. The relationship between the tectonic features surrounding Tepev Mons and stresses associated with magma chamber inflation are also examined through finite element analysis. Using topography data to model the shape of the volcano, we determine that a horizontally ellipsoidal or tabular reservoir at a range of depths from approximately 20 to 40 km can satisfy the locations of graben formation observed in Magellan images. These results imply a shift in volcanic style within Bell Regio from an early phase of broad, low shield formation to later steep-sided, more centralized edifice development. Such changes are consistent with an increase in the thickness of the lithosphere over time.

1. Introduction

Geophysical analyses of the tectonic features associated with the Venus highlands and major volcanoes provide important insight into the relationship between volcanic and tectonic processes and the stress state of the venusian crust over time. Bell Regio is unique relative to many of the other volcanic highland regions on Venus, such as Western Eistla or Dione Regiones [*Senske et al.*, 1992], in its apparent lack of rift zones dissecting the topographic swell. Most large Venus volcanoes also exhibit radial tectonic structures on their flanks, and typically lack the circumferential graben which surround volcanoes on Earth and Mars, indicating lithospheric flexure [*Comer et al.*, 1985; *McGovern and Solomon*, 1992]. Tepev Mons and Nyx Mons (provisional name) exhibit both the radial tectonic features associated with other venusian edifices and numerous distinct concentric graben [*Campbell and Rogers*, 1994].

To understand the geophysical evolution of Bell Regio, this study examines the structural features associated with the major volcanoes using Magellan synthetic aperture radar (SAR) images and altimeter measurements of topography. First, we analyze the regional stress field in Bell Regio based on the style and distribution of tectonic features in the region. Next we examine structural features we believe to be a consequence of lithospheric flexure due to volcanic loading. Analytical models for the formation of similar features on Earth and other planetary surfaces are examined, and a model for the stress regime and formation of tectonic structures within Bell Regio is developed. This analysis of lithospheric flexure and associated deformation models the volcano as an axisymmetric load with a Gaussian mass distribution on an elastic plate of variable thickness, and incorporates criteria for tensile and shear failure. Finally, the relationship between the tectonic features

[1] Currently at Center for Earth and Planetary Studies, Smithsonian Institution, Washington, D.C.

Copyright 1998 by the American Geophysical Union.

Paper Number 98JE00585.
0148-0227/98/98JE-00585 $09.00

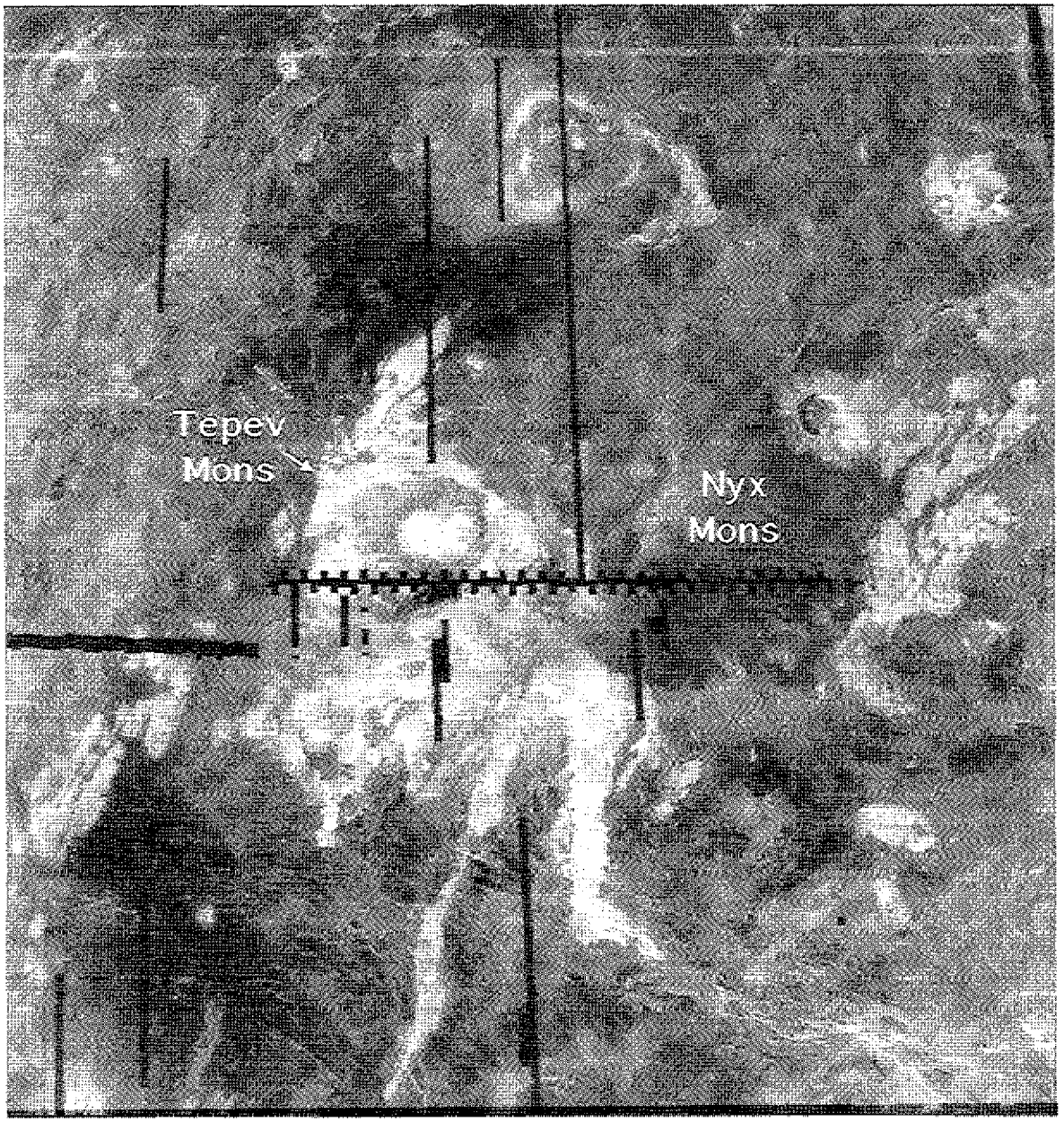

Figure 1. Magellan SAR image of Bell Regio. Resolution is approximately 1.2 km. For scale, the large caldera on Tepev Mons, the prominent central edifice in the image, is approximately 30 km.

associated with the Tepev Mons edifice and stresses associated with magma chamber inflation is examined through finite element analysis.

2. Regional Stress Regime

Analysis of regional stresses provides a framework for understanding smaller-scale tectonic features within the highland. As indicated above, this region lacks rift zones; however, large-scale tectonic deformation is exhibited by tessera blocks which surround the major volcanic edifices (Figure 1) [*Campbell and Rogers*, 1994]. Tessera are generally the stratigraphically oldest units in this region and preserve a record of periods of intense tectonic deformation. The fractures within some blocks are irregularly oriented, but the prevailing fracture patterns within the tessera regions trend SW-NE. The preexisting tessera plateaus are thought to be regions of thickened crust [*Bindschadler and Head*, 1991] and may have inhibited lateral spreading and the formation of major rift zones during the early period of highland formation. If the stresses that governed the formation of the SW-NE tessera blocks still existed at the time the volcanic edifices formed, similar trends in the subsequent volcanic and tectonic features might be observed. However, although some of the Nyx Mons lava flows trend SW-NE, little direct evidence of significant SW-NE fracture patterns exists. This implies that the formation of Tepev Mons and Nyx Mons postdate the regional stress regime which produced the tessera or that stresses in the regions that lack fractures did not exceed the lithospheric failure criteria.

Plains regions surrounding Bell Regio are next in the stratigraphic sequence after the tessera and may be divided

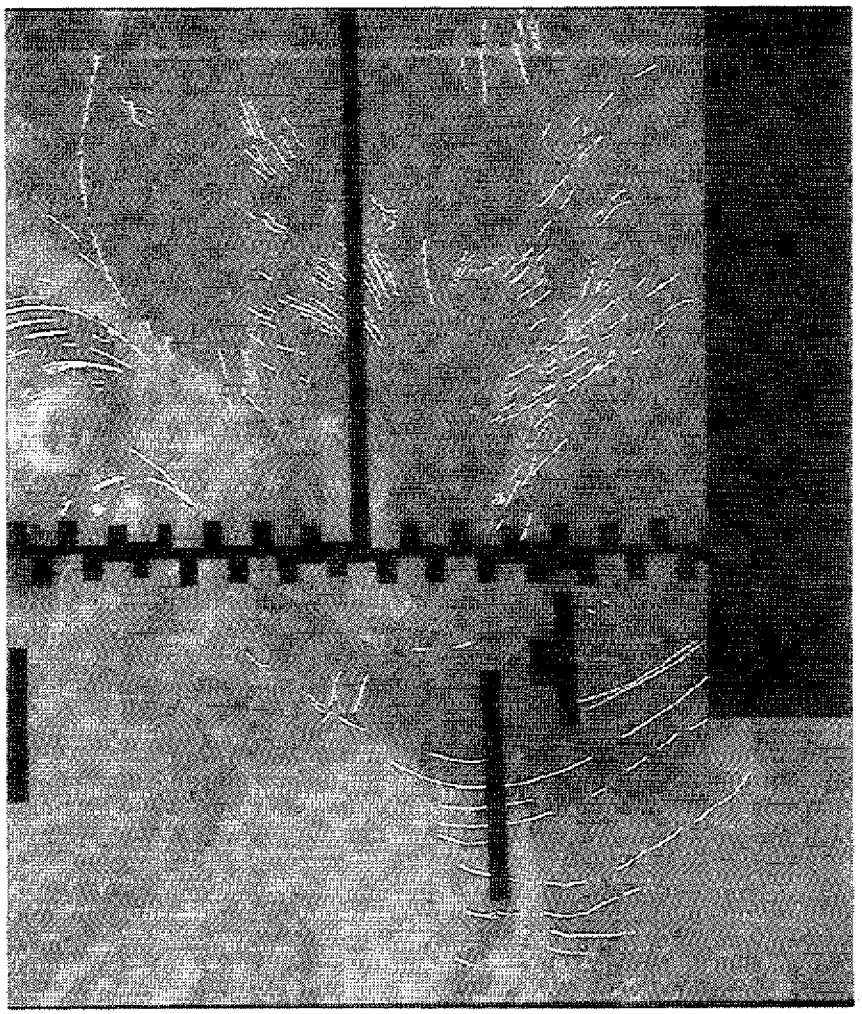

Figure 2. Magellan SAR image of Nyx Mons with concentric fracture map overlay, centered at approximately 29.9°N, 48.5°E. Note the radial chains of pit craters and concentric fractures surrounding the edifice outlined in the image.

into at least three distinct units: bright plains, dark plains, and ridged plains [*Campbell and Rogers*, 1994]. The ridged plains are the oldest of these units and record an intense period of deformation with ridges and graben oriented SE-NW and SW-NE. The bright and dark plains are less deformed than the ridged plains or the tessera, with deformation primarily represented by SE-NW trending fractures. Since the lava flows from the major volcanic edifices in this region embay the tessera, superpose most of the plains units, and do not contain major deformation patterns, it is reasonable to conclude that the last large volcanic events in this region postdate the regional stress regime which produced the tessera and ridged plains. These volcanic units thus record more recent localized stresses in the region and are the subject of the next sections.

3. Lithospheric Flexure and Nyx Mons

The oldest volcanic edifice within Bell Regio is Nyx Mons, a feature characterized by a wishbone pattern of ridges and gentle flank slopes. The inner region contains a central bulge and radial chains of pit craters [*Campbell and Rogers*, 1994]. Surrounding the edifice to the east, south, and northwest are large sets of circumferential fractures, which are the main focus of this section (Figure 2). Figure 3 illustrates the topography of Nyx Mons and surrounding regions. This edifice rises approximately 1 km above the surrounding apron of flows; the central bulge and wishbone ridges contain the highest elevations of the feature at approximately 6053.5 km. Slopes on the southern flanks of the edifice are generally 1° - 2°, grading into slopes less than 0.5° continuing southward, corresponding to the flow apron that typically surrounds volcanoes on Venus [*McGovern and Solomon*, 1995]. It is in this gently sloping region that the most prominent concentric graben occur. Detailed structural mapping of these features indicates that the innermost concentric graben occur at a radial distance of approximately 280 km from the center of the edifice, while the outer radius of these features lies at approximately 470 km. A 500-m change in elevation occurs between these two radii. The most prominent volcanic flow fields in the region (the youngest flows of Nyx Mons) emanate from these concentric fractures [*Campbell and Rogers*, 1994].

3.1. Models of Lithospheric Flexure

The distribution of fractures around large volcanic loads is an important indicator of the stress state and effective thickness of the elastic lithosphere. Comparing the tectonic features formed in response to large volcanic loads on various

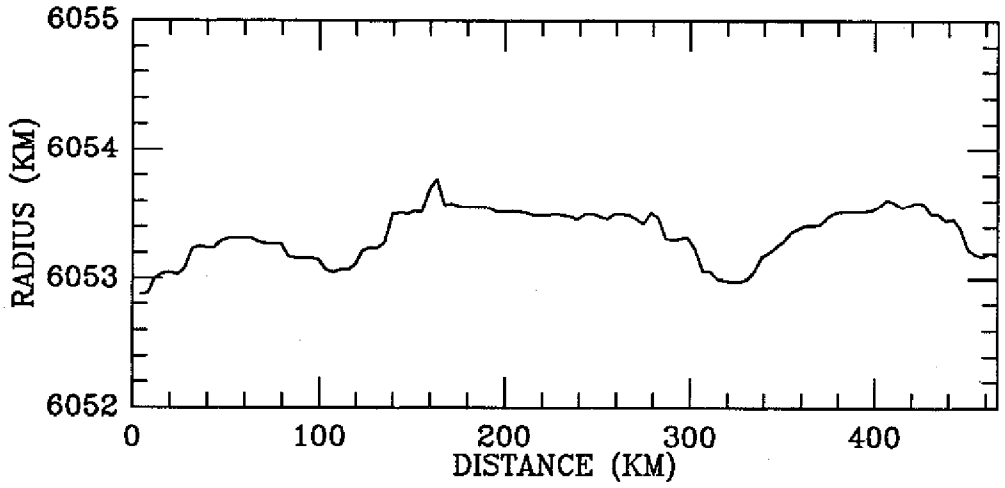

Figure 3. Topographic profile through Nyx Mons trending approximately west to east. Note the higher elevated ridges and central regions.

planetary surfaces has provided important constraints on the relative lithospheric thicknesses on Venus, Earth, Mars, and the Moon [e.g., *Melosh*, 1976, 1978; *Comer et al.*, 1985; *Hall et al.*, 1986; *McGovern and Solomon*, 1993]. In these analyses, graben form concentric to a load as a result of surficial extensional bending stresses associated with lithospheric flexure. If the lithosphere is extremely thick or rigid, then the stress field is dominated by compressional forces due to the volcano [*Artyushkov*, 1973; *Fleitout and Froidevaux*, 1983].

This analysis of lithospheric flexure and associated deformation models the two major volcanoes within Bell Regio as axisymmetric loads with Gaussian mass distributions on an elastic plate, following the analysis of *Melosh* [1978] of the mechanics of lunar mascon loading. Deviations of the actual load from axisymmetry are a second-order effect [*Comer et al.*, 1985]. *Melosh* [1978] analyzed load-related stresses and deformation and determined that the tectonic pattern predicted by this model, with increasing radial distance from the center of the load, included a proximal zone of radial thrust faults followed by strike-slip faults, all surrounded by concentric normal faults. Although the zone of strike-slip faulting is not readily observed surrounding the lunar mascons, they suggested that some of the ridges surrounding lunar maria might be evidence of strike-slip motion. *Golombek* [1985] proposed that the lack of observed strike-slip faults can be explained by the fact that fault nucleation occurs at subsurface interfaces, though this does not account for the absence of such features in regions that most likely lack discrete subsurface layering.

In an analysis of the formation of large volcanic loads on Mars by *McGovern and Solomon* [1993], time-dependent effects on the predicted failure mechanisms of the growing load were considered. They determined that the zone of strike-slip faulting is not observed because it either occurs in a region that had previously formed normal faults (the normal faults are reactivated), or that they form and are buried by subsequent deposits. The fractures considered in our analysis occur on the youngest volcanic flows; therefore this analysis considers their formation as a late stage event and is not concerned with the growing load. However, our treatment of the lithosphere as an elastic plate inherently supposes that stresses due to the growing edifice did not pervasively fracture the lithosphere. In a more recent analysis, *McGovern and Solomon* [1997] attribute the absence of topographic moats and concentric normal faulting surrounding large Venus volcanoes to masking by lava flows from the central edifice. In their model, the stresses in this moat fill are too low to induce failure.

Schultz and Zuber [1994] addressed the paradox of the existence of an annular zone of strike-slip faults around prominent loads predicted in previous models, evidence for which is rarely found on planetary surfaces. In their model, the discrepancies between the observations and the model predictions result from other considerations significant in fault analysis: the neglect of stress magnitudes and reliance only on stress trajectories, and the identification of first failure. When rock strength, stress differences, stress geometries or stress state at the onset of failure and load evolution are taken into account, their model predicts that concentric normal faults and joints (as opposed to strike-slip faults) occur at or near the surface surrounding loads. Rock strength is significant in determining the stress level when the first fractures occur. Their model, which examines the importance of failure mechanisms such as tensile cracking near surface regions and varying values of Young's modulus, was experimentally verified by *Williams and Zuber* [1995]. The analysis below uses the general solutions described in the *Melosh* [1978] model but also incorporates these failure criteria.

3.2 Modeling Volcanic Loads

This study analyzes the volcanic edifices and associated stresses in Bell Regio by modeling the two major loads as Gaussian distributions on an elastic plate following *Melosh* [1978]. The general solution to the stress field is given by *Melosh* [1978] as

$$\sigma_{zz} = \pm\rho_c g z + J_0(kr)\,[(A + Cz)\cosh kz + (B + Dz)\sinh kz] \quad (1)$$

$$\sigma_{rr} = \pm\kappa\rho_c g z \pm\left(J_0(kr) \pm \frac{J_1(kr)}{kr}\right)[(A + Cz)\cosh kz + (B + Dz)\sinh kz] + \frac{2}{k}\left(J_0(kr) \pm \frac{(1\pm\nu)}{kr} J_1(kr)\right)[D\cosh kz + C\sinh kz] \quad (2)$$

$$\sigma_{\phi\phi} = \pm\kappa\rho_c g z \pm \frac{J_1(kr)}{kr}\,[(A + Cz)\cosh kz + (B + Dz)\sinh kz] + \frac{2}{k}\left(\nu J_0(kr) + \frac{(1\pm\nu)}{kr} J_1(kr)\right)[D\cosh kz + C\sinh kz] \quad (3)$$

$$\sigma_{rz} = J_1(kr)\,[(A + Cz + \frac{D}{k})\sinh kz + (B + Dz + \frac{C}{k})\cosh kz] \quad (4)$$

$$\sigma_{r\phi} = \sigma_{z\phi} = 0 \quad (5)$$

where $J_1(kr)$ and $J_0(kr)$ are Bessel functions, σ_{zz} is the vertical stress, σ_{rr} is the radial stress, $\sigma_{\phi\phi}$ is the hoop (tangential) stress, σ_{rz} is the shear stress, σ_n is the normal stress, r is the radius from the center of the load, z is the depth in the plate, k is the wave number, and ν is Poisson's ratio. Because the total stress is sought in this analysis, a term for the confining pressure ($\kappa\rho_c gz$) is added to the above stresses where κ is the ratio of horizontal to vertical overburden [*Banerdt*, 1988]. The vertical stress at the surface, and the lack of shear stress at the surface or base are indicated by the following boundary conditions:

$$\sigma_{zz}(z = 0, r) = bJ_0(kr) \quad (6)$$

$$\sigma_{rz}(z = 0, r) = \sigma_{rz}(z = H, r) = \sigma_{zz}(z = H, r) = 0 \quad (7)$$

In this analysis, the vertical load is represented by

$$w = \rho_m gT \quad (8)$$

where ρ_m is equal to its density, T is its height at $r = 0$, and g is gravitational acceleration. According to *Anderson* [1951], concentric normal faulting will occur in the region defined by positive σ_{rr} and $\sigma_{\phi\phi}$ and maximum σ_{rr}.

In order to distinguish the likely mechanism for initial lithospheric failure, we have incorporated into this formalism the following rock failure criteria: a Griffith criterion for tensile failure and the Byerlee criterion for shear failure [*Schultz and Zuber*, 1994]. Specifically, applying stress to a fractured rock will cause frictional sliding along the fractures prior to reaching the level required to cause brittle failure of the rock mass. This relationship, referred to as Byerlee's law, is given by [*Brace and Kohlstedt*, 1980]

$$\begin{aligned} \tau &= 0.85\,\sigma_n & 3 < \sigma_n < 200\ \text{MPa} \\ \tau &= 60 \pm 10 + 0.6\,\sigma_n & \sigma_n > 200\ \text{Mpa} \end{aligned} \quad (9)$$

The Griffith criteria for brittle failure states that fracture occurs at a given stress according to

$$\sigma_t = (2AE / \pi c)^{1/2} \quad (10)$$

where 2c is the length of the pre-existing crack, A is the surface energy, E is the Young's modulus, and σ_t is the applied tensile stress [*Price and Cosgrove*, 1990].

Table 1. Fixed Parameters Used in Modeling Nyx Mons

Parameter	Description	Value
g	gravitational acceleration	8.6 m s^{-2}
ρ_m	load density	3000 kg m^{-3}
T	load height	1 km
κ	horizontal/vertical overburden	0.5
ν	Poisson's ratio	0.33
ρ_c	lithosphere density	3300 kg m^{-3}

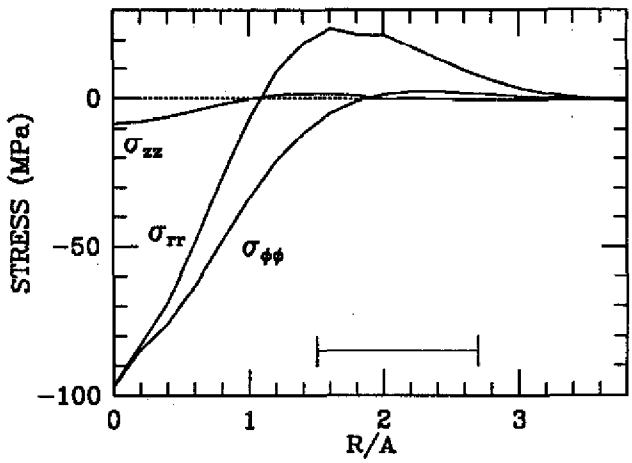

Figure 4. Plot of elastic surface stresses resulting from the Nyx Mons load with a lithospheric thickness of 50 km. Negative stresses are compressional and positive stresses are extensional. The bar represents the zone of fracturing observed in the images and corresponds well to the R/A range of 1.5-2.7 resulting from the model.

3.3. Nyx Mons Modeling Results

In this analysis, an analytic model was used to determine the stress field and predict the spatial distribution of faulting on the lithosphere surrounding Nyx Mons. The predictions were then compared to the observed fault distributions, thereby constraining the properties of the lithosphere that supports the volcano. Fifteen cases, with varying lithospheric thickness and Young's modulus, were considered in this analysis of Nyx Mons to determine which most closely corresponds to the observed fracture patterns. The fixed parameters are given in Table 1.

In the first seven cases, the effects of varying the lithospheric thickness between 30 and 70 km were examined. The diameter of the feature was defined to be the distance at which the topography of the edifice merged with the surrounding plateau. Since Nyx Mons is an irregularly shaped "wishbone" feature, minimum and maximum values for the load extent were also examined. The maximum diameter, corresponding to the feature's N-S extent, is 350 km, and the minimum diameter, corresponding to the edifice's E-W extent and an idealized circular shape for the feature, is 270 km. These diameters correspond to halfwidths of 175 and 135 km, respectively. The deviation of the load from a Gaussian shape is not significant.

The next cases examined the effects of varying Young's modulus. In-situ measurements of elastic moduli can be up to an order of magnitude lower than laboratory measurements [*Cullen et al.*, 1987], so we examined the effect of reducing Young's modulus by an order of magnitude (from 10^{11} to 10^{10} Pa) while varying the load halfwidth and the lithospheric thickness. Next we examined the effect of an increase in Young's modulus (to 10^{12} Pa). This situation may represent the effective Young's modulus of a rock containing closed cracks [*Jaeger and Cook*, 1979] although it's uncertain that this effect would increase E by an order of magnitude. We consider this value to be an upper limit on E.

The effect of increasing the lithospheric thickness shifts the range of concentric normal faulting to slightly higher val-

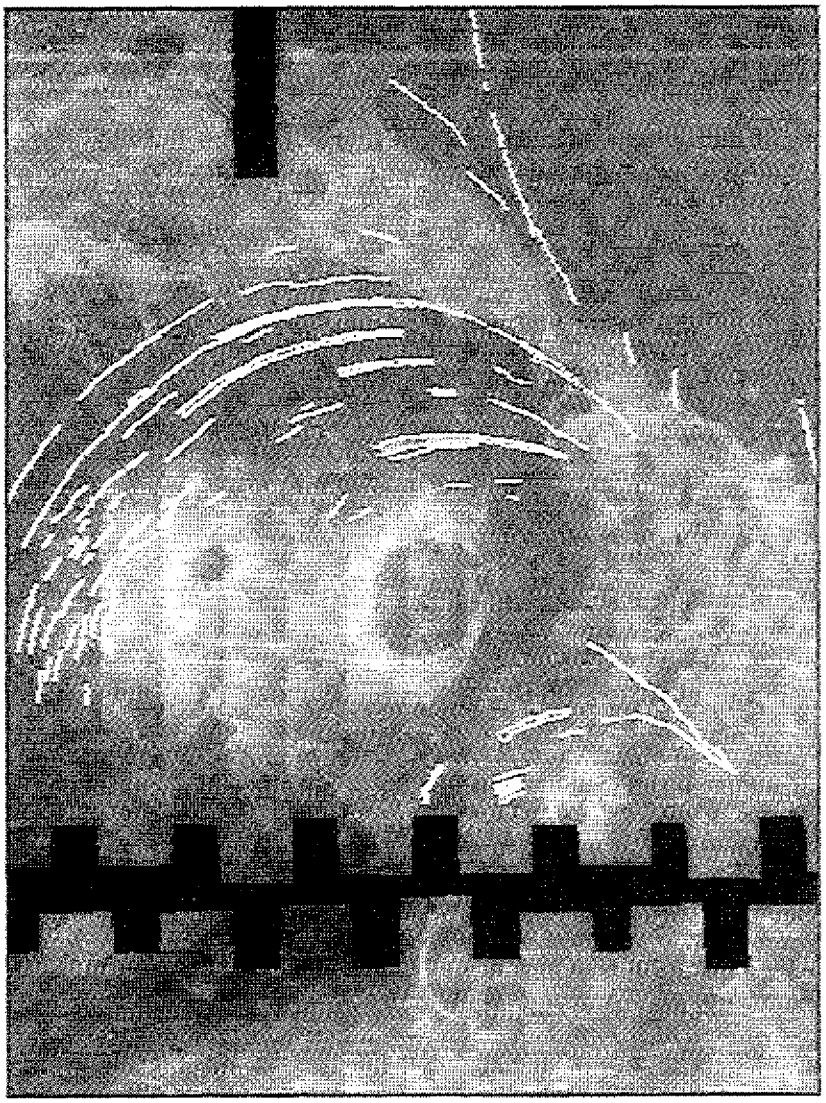

Figure 5. Magellan SAR image of Tepev Mons with fracture map overlay. Note the prominent fractures concentric to the volcano. For scale, the largest caldera on Tepev Mons is approximately 30 km in diameter.

ues of R/A (normalized radial position, where A is the halfwidth of the load), while decreasing the size of the load causes a small increase in the maximum σ_{rr} and the range of R/A for graben formation. Decreasing Young's modulus decreases σ_{rr} and the R/A range for graben formation, while increasing E has the opposite effect.

The inner and outer radii for the concentric faults (280 and 470 km) correspond to an R/A range of approximately 2.0 - 3.5 if A = 135 km and an R/A range of 1.6 - 2.7 if A = 175 km. Figure 4 illustrates the results of the best solution that produces concentric normal faulting in the range of 1.5 - 2.7. Total stress (MPa) is plotted against R/A. Individual points are plotted on the σ_{rr} curve. These results indicate that for the parameters used in this analysis, a lithospheric thickness of 50 km, $E=10^{11}$, and load halfwidth of 175 km best describes the conditions at Nyx Mons at the time of the formation of the concentric graben.

4. Edifice Stresses and Tepev Mons

Tepev Mons is a prominent volcanic shield within Bell Regio thought to be younger than the large volcano Nyx Mons discussed above [*Campbell and Rogers*, 1994]. It rises approximately 5 km above the surrounding plains and is characterized by relatively steep slopes (20° - 40°) near the summit region. The steepest slopes occur along the eastern flank of the volcano (Figure 5). Two large (11 and 31 km diameter) calderas superpose the summit region. The northern flank is characterized by prominent fractures and coalesced chains of pit craters concentrically distributed around the main peak and calderas. In this section we consider the origin of tectonic features on Tepev Mons, beginning with a test of the lithospheric flexure model used above and concluding with a comparison between terrestrial volcanic deformation patterns and the Venus observations.

4.1. Modeling of Tepev Mons Concentric Fractures

In preliminary analyses by *Solomon et al.* [1992] it was postulated that the concentric graben north of Tepev Mons may have resulted from lithospheric flexure due to the volcanic load. To test this hypothesis, an analysis similar to the one described above for the formation of the concentric graben surrounding Nyx Mons was performed for the Tepev Mons load.

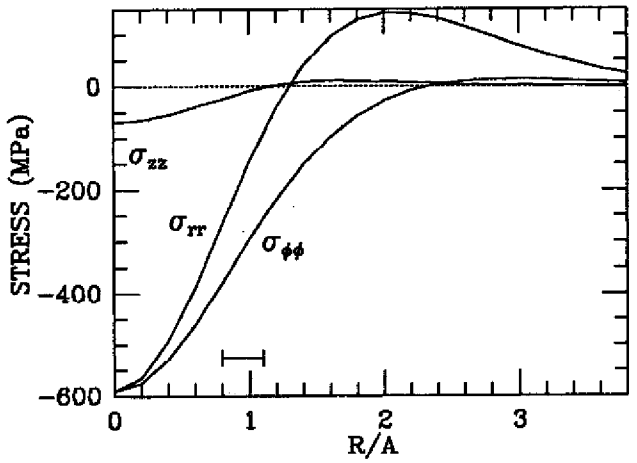

Figure 6. Plot of elastic surface stresses resulting from modeling the Tepev Mons load with a lithospheric thickness of 30 km. The bar represents the zone of fracturing observed in the images. Unlike the Nyx Mons case, this region does not correspond to the R/A range of 1.5-2.5 resulting from the model.

Five cases were examined in which the lithospheric thickness varied from 20 to 60 km. The results of the model for the case of a 30-km-thick lithosphere are illustrated in Figure 6.

Structural mapping of concentric graben around Tepev Mons indicates that these features occur at inner and outer radial distances of 65 and 90 km, respectively. With a halfwidth for the load of 80 km based on topographic profiles across the edifice (Figure 7), this corresponds to R/A values ranging from 0.8 to 1.1. However, results of the model indicate that maximum extensional stress occurs at R/A of 1.5 to 2.5. This region corresponds to the approximate location of a possible topographic moat north of Tepev Mons (R/A = 1.8) which has been discussed by several authors [*Janle et al.*, 1988; *Solomon and Head*, 1990; *McGovern and Solomon*, 1992; *Campbell and Rogers*, 1994] (Figure 8). The effective elastic thickness based on the location of this volcanically flooded moat yielded a preliminary value of approximately 10 km [*McGovern and Solomon*, 1992]. However, the lava flow which fills this moat has a high surface roughness [*Campbell and Rogers*, 1994] which may have prevented the Magellan altimeter from acquiring an accurate surface response, which could result in spurious range measurements. Hence the minimum elevation of this potential moat is difficult to constrain. Assuming the flow is contained within the lowest region, the approximate center of the moat would correspond to an R/A value of 1.8, almost at the center of the range of maximum extension predicted in our models using a lithospheric thickness of 30 - 50 km. This result is supported by recent studies of gravity-topography relationships which yield elastic thickness estimates for this region in the range of 30-50 km [*Smrekar*, 1994].

There is thus evidence for lithospheric bending associated with Tepev Mons, but the results of our model indicate that this flexure is not the likely cause of the prominent concentric graben which occur on the steep northern flanks, close to the center of the load. Similar features are observed on the flanks of Pavonis and Arsia Mons, two large shield volcanoes on Mars [*Comer et al.*, 1985]. Comer et al. studied the tectonic features associated with large volcanic loads on Mars and determined that the concentric graben on Pavonis and Arsia which lie close to the center of the load may be concentric extensional fractures formed during the evolution of the caldera rim as magma was withdrawn or solidified, producing an annular ring of faults. Another cause may have been topographic stresses and gravitational spreading, which resulted in extensional faults on the flanks of the shield [*McGovern and Solomon*, 1993]. The concentric graben may also reflect zones of weakness inherited from flexural stresses during an early stage of volcano growth. In the next section we examine some of these mechanisms in more detail and discuss possible terrestrial analogs to understand if stresses within the Tepev Mons edifice may have produced the observed circumferential fractures.

4.2. Models of Edifice Deformation

As discussed above, the free surface of a volcanic edifice may undergo tectonic deformation as a result of several mechanisms: inflation and doming due to subsurface injection of magma, deflation associated with caldera collapse, and gravitational relaxation which may lead to slumping of material along the flanks. The mechanical behavior and overall morphology of a volcanic shield generally results from the interaction of all these processes. However, gravitational collapse and slump-

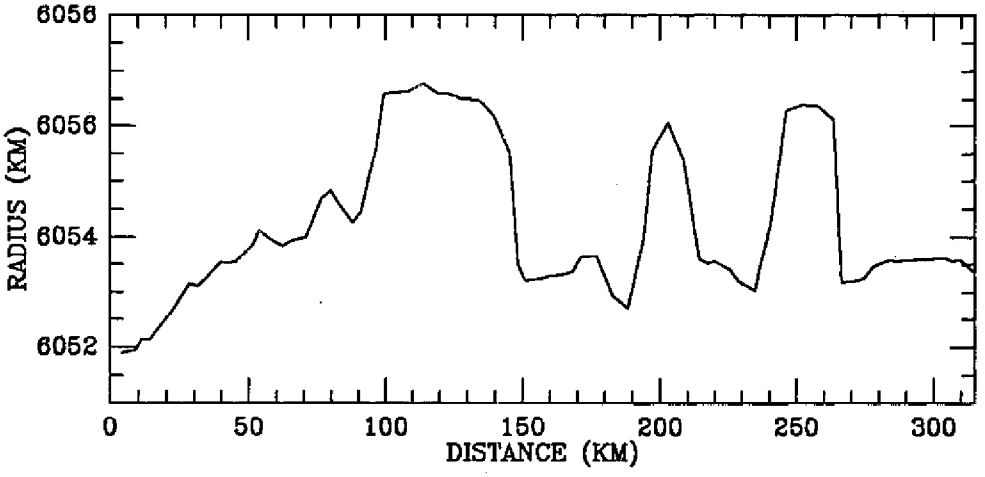

Figure 7. Topographic profile through Tepev Mons trending approximately NW to SE. The two peaks centered at approximately 200 and 250 km represent small, steep volcanoes on the SE flanks of Tepev Mons.

Figure 8. Magellan SAR image of lava flow north of Tepev Mons, thought to be confined within a topographic moat. Tepev Mons is off the image to the southeast.

ing of the flanks may be less significant for venusian edifices due to their relatively gentle profiles and limited vertical extent [*Head and Wilson,* 1992]. Therefore the major forces affecting the overall morphology of Venus volcanoes may be related to stresses associated with the evolution of a magma reservoir and internal dike propagation. Several authors have examined the surface deformation associated with stresses that arise from the inflation and deflation of a subsurface magma chamber. A period of uplift and swelling of the edifice may occur due to the inflation of such a magma chamber and the associated injection of dikes and sills. Deflation, which may lead to caldera collapse, results as rift eruptions occur along the flanks or as intrusions occur into new regions within the volcano [*Dieterich and Decker*, 1975; *Marsh*, 1984].

In early models of magma chamber deformation the chamber was represented by a point source in an elastic half space, or by magma reservoirs that were spherical and small in comparison to their depth [*Anderson,* 1935; *Mogi*, 1958]. However, these point source models applied accurately only to stresses at large distances from the chamber. Later models represented the magma reservoir as a finite source and were able to more accurately determine near field (shallow source) stresses [*Ryan,* 1988]. *Dieterich and Decker* [1975] determined that the early analytical approaches predicted generally similar surface deformation, regardless of the actual model used and that these models did not predict the ratio of horizontal to vertical surface movements observed near summit regions. They were among the first to use a finite element method, enabling them to model summit deformations and rift zone intrusions using a variety of shapes and depths for the magma reservoir. *Dieterich and Decker* [1975] also observed a relationship between flank eruptions and the systematic inflation and deflation of the summit reservoir; flank eruptions occur as magma is transported vertically to a shallow storage zone beneath the summit followed by lateral transport of magma from the summit reservoir to the flanks by dikes. *Zuber and Mouginis-Mark* [1992] examined the tectonic responses associated with the evolution of the caldera on Olympus Mons, Mars. They used a linear elastic finite element model to determine the range of magma chamber geometries and pressures that could produce the observed tectonic pattern. Specifically, the ridges and graben which formed from subsidence of the caldera floor during deflation of the magma chamber were used to provide constraints on the dimensions, depth and pressures associated with the subsurface reservoir. They determined that the surface stress distribution is relatively insensitive to the details of the shape of the magma chamber and is very sensitive to its depth.

4.3. Numerical Modeling of Edifice Deformation

In this section we examine whether the concentric graben observed on the flanks of Tepev Mons could be due to stresses within the edifice. To understand the nature of the stress state of the edifice, we constructed an axisymmetric finite element model to calculate the elastic stresses within the volcano and to examine the relationship between these stresses and the observed tectonic features. Following a model previously employed in the study of caldera subsidence [*Zuber and Mouginis-Mark,* 1992] we analyzed the stresses associated with variations in a magma reservoir. However, while the *Zuber and Mouginis-Mark* [1992] analysis modeled the deflation of the magma chamber and the resulting caldera structures, this model is concerned with the inflation of the magma chamber and the associated stresses on the flanks of the volcano. Deflation and resulting deformation within the Tepev Mons calderas may have also occurred during its history, however structures within the calderas of Tepev Mons can not be resolved, most likely due to the presence of a fine grained surficial deposit [*Campbell and Rogers*, 1994]. We used the finite element program TECTON [*Melosh and Raefsky,* 1981] to develop a linear elastic model of the stresses and displace-

Table 2. Parameters Used in Finite Element Modeling of Tepev Mons

Parameter	Value
Density	3000 kg m^{-3}
Young's Modulus (within chamber)	10^9 Pa
Young's Modulus (outside chamber)	10^{11} Pa
Poisson's ratio	0.33

ments associated with the edifice and underlying crust and mantle.

In order to improve the accuracy of the finite element representation of the volcano, we extracted a representative topographic profile for Tepev Mons from the Magellan global-average (5.4-km resolution) data set. The model grid was then constructed to conform to this profile shape along the upper surface. Given that Tepev Mons has significant changes in slope along its flanks, this method permitted a more realistic assessment of the role of local topography on the final stress field. The profile we used for the Tepev Mons volcano was taken from the approximate center of the larger eastern caldera (29.6°N, 45.6°E) and extended to the northwest. From the start of this profile, the zone of concentric graben formation begins at approximately 40 km and extends to approximately 115 km. Any additional graben at greater distances may have been obscured by later lava flows.

The magma reservoir was modeled as a simple chamber in which inflation occurs as a distribution of outward directed radial forces at specified nodes, with the force magnitude equal to 1×10^9 kg m s^{-2} (1000 MPa). Varying the force magnitude affected the magnitude, but not the distribution, of surface stresses. The model allows analysis of varying magma chamber depth, size, and shape, as well as the density, Poisson's ratio, and Young's modulus of the magma and country rock. The parameters most typically used are listed in Table 2.

Figure 9 illustrates an example of the axisymmetric finite element grid used in this analysis containing 8238 nodes and 8181 elements, with a grid size of 100 km by 300 km. This case models a spherical magma chamber which has 107 elements, lies at a center depth, D, of 30 km, and has dimensions of $R_X = R_Y = 16$ km. The left boundary is a symmetry axis along which horizontal displacements vanish. At the bottom boundary of the grid, at depths much larger than the level of the chamber, vertical displacements vanish, while at large radial distances (right boundary) both horizontal and vertical displacements vanish. Figure 10 illustrates the surface stresses resulting from this analysis.

The resulting variations in the stress field were examined and the model results were compared with our observations from Magellan images. Specifically, the innermost location of predicted concentric graben formation is defined by the point at which σ_{rr} crosses from negative (compression) to positive (extension) in the finite element results, following methods used in previous studies [*Comer et al.*, 1979; *Zuber and Mouginis-Mark*, 1992]. We also considered a case with no magma chamber to analyze stresses due solely to the volcano, and found relatively small load-induced surface stresses in the vicinity of the summit that were easily overwhelmed by the effects of even a small magma chamber. However, this analysis does not account for edifice stresses from other sources such as lithospheric flexure, which would tend to add horizontal compression in the upper lithosphere and may inhibit the transmission of extensional stresses to the surface [*McGovern and Solomon*, 1993]. Thus the depth of burial for any given magma chamber must be shallower to produce the observed graben than for a scenario without flexural stresses. Likewise, the observable distribution of fractures may have been altered due to burial by superposing flows [*McGovern and Solomon*, 1997]. Specifically, the burial of the innermost fractures near the summit region would increase the horizontal radius of the σ_{rr} crossover, and bias the prediction of the magma chamber radius to larger values. Burial of innermost graben would also bias the depth prediction to larger values, since graben formation moves outward with increasing depth to the chamber. Neglecting these additional potential factors thus biases our predictions toward larger chamber depths, so our analysis places an upper bound on the depth of burial.

4.4 Results

In order to constrain the likely magma chamber geometry, we varied alternately the depth, size, and shape of the model reservoir. Numerous chamber geometries were examined (approximately 90 total variations), from a spheroid with vary-

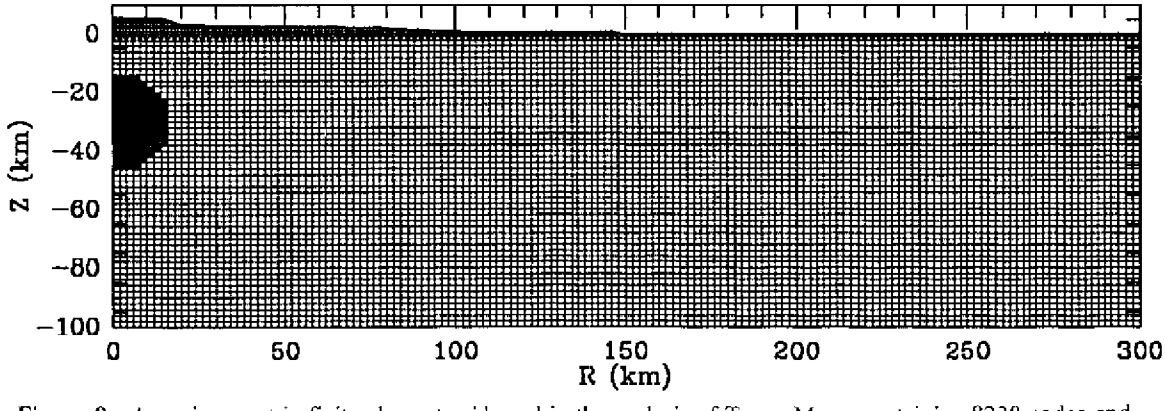

Figure 9. An axisymmetric finite element grid used in the analysis of Tepev Mons, containing 8238 nodes and 8181 elements, with a grid size of 100 km by 300 km. The magma chamber in this example lies at a center depth (D) of 30 km, and has dimensions of $R_x = 16$ km (horizontal radius), and $R_y = 16$ km (vertical radius).

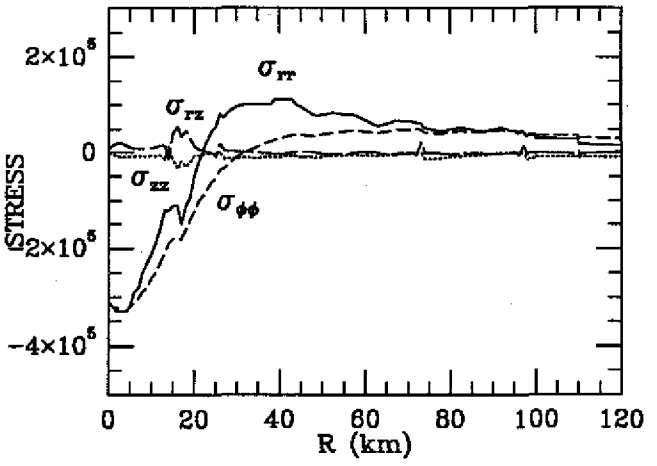

Figure 10. Elastic surface stresses resulting from the inflation of a spherical magma chamber beneath Tepev Mons, illustrated in Figure 9.

ing radii to ellipsoids with varying horizontal and vertical axes. Table 3 illustrates results from several of these models. As the vertical dimension (R_Y) of the chamber increases relative to the horizontal dimension (R_X) (a vertically elongate ellipsoid), or the depth to the chamber becomes shallower, the stresses become more concentrated towards the center of the load and the zone of extension (graben formation) moves inward. It is obvious from Table 3 that neither spherical chambers nor ellipsoidal magma bodies comparable in size to the summit caldera can produce the required stress field within a range of reasonable depths.

The 40-km crossover point can be accommodated most easily by a tabular magma chamber 44-52 km in radius, approximately 8 km in maximum thickness, over a range of depths from 18 to 36 km. The tradeoffs between shape and depth are illustrated in Table 3. The thickness of the chamber has less of an impact on the location of the crossover point than the width and depth of burial. The small changes in crossover point with changing thickness reflect the varying

Table 3. Variations in σ_{rr} Crossover Point (From Compressional to Extensional Regime) With Changes in D (Depth to Center of Chamber), Rx (Horizontal Radius), and Ry (Vertical Radius)

D_{center}, km	Rx, km	Ry, km	Crossover σ_{rr}, km
Spherical Chambers:			
-15	16	16	16
-30	16	16	22
-50	16	16	26
Ellipsoidal Chambers:			
-20	10	20	16
-50	10	20	19
-40	20	30	27
-50	20	30	31
Tabular Chambers:			
Shallow:			
-18	45	4	35
-18	52	4	40
-18	60	4	46
-18	66	4	49
Intermediate:			
-28	56	4	45
-28	48	4	40
Deep:			
-36	48	4	42
-36	44	4	40
Sensitivity to Thickness:			
-22	62	2	46
-22	62	4	48
-22	62	6	47
-22	62	8	45

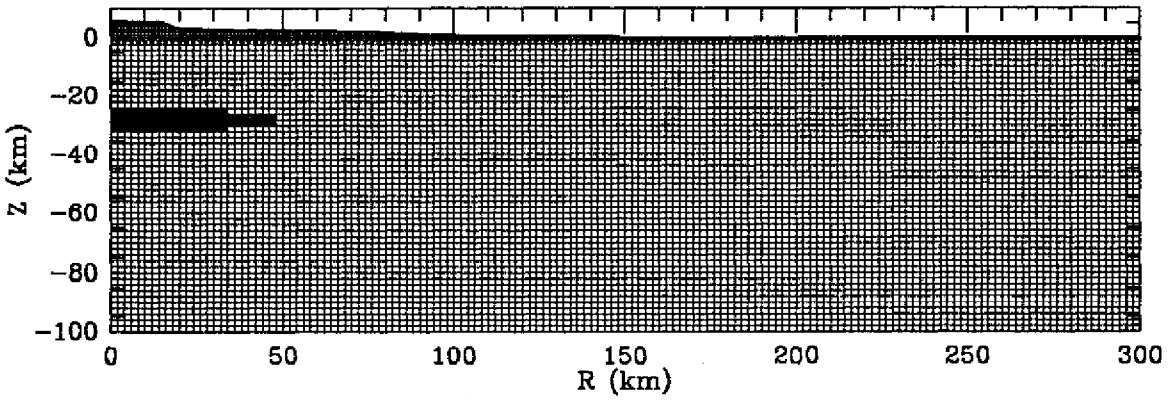

Figure 11. Axisymmetric finite element grid for a solution of Tepev Mons edifice stresses with a magma chamber at an intermediate depth. The magma chamber, representing a sill-like intrusion, lies at a center depth (D) of 28 km, and has dimensions of $R_x = 48$, and $R_y = 4$.

distance to the surface from the upper boundary of the chamber. The width of the reservoir is inversely correlated with the depth, such that more narrow "sills" may produce the required stress field as the centerline depth increases. Note, however, that the surface stress magnitude declines with increased chamber depth, so a shallow chamber may be more likely to create observable fractures.

Our results indicate that the circumferential graben occurring on the flanks of Tepev Mons could be the result of edifice stresses caused by a sheet-like or tabular magma reservoir. Figures 11 and 12 illustrate the results of this solution for an intermediate chamber depth (28 km) with a horizontal radius of 48 km and a vertical radius of 4 km. This sill-like intrusion may possibly have fed smaller magma chambers at shallower depths. However, without better resolution of the structure within the calderas, further analysis is not possible. Our analysis of Tepev Mons shows that the observed spatial distribution of graben may be attributed to stresses caused by magma chamber inflation, and therefore no inference of lithospheric thickness can be made from these graben locations. However, our earlier analytical model of Tepev Mons flexure based on the possible location of a topographic moat may provide constraints on the thickness of the elastic lithosphere.

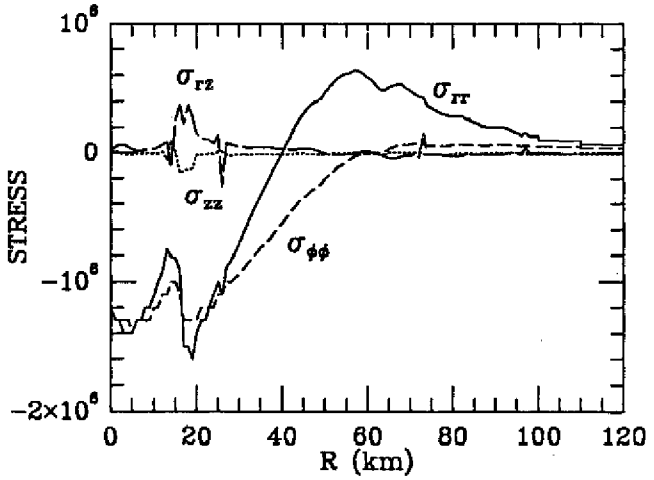

Figure 12. Elastic surface stresses resulting from the inflation of a horizontally elongate (sill-like) magma chamber beneath Tepev Mons, illustrated in Figure 11. The bar represents the region of fracturing observed in the Magellan images.

5. Discussion and Conclusions

In this study, the nature of the stress state and lithospheric structure of Bell Regio have been examined. The style and distribution of tectonic features associated with the volcanic loads in Bell Regio were analyzed in an attempt to understand the regional stresses which produced these features. A complex history of stress regimes is illustrated through the various structural features associated with several different geologic terrains. The oldest units in the region, SW-NE trending tessera blocks, provide constraints on the early regional stress trajectories. These regional stresses do not appear to have affected the emplacement of the large volcanic edifices, Tepev Mons and Nyx Mons.

To quantify the stress regime in Bell Regio we have applied analytical models for the formation of similar structures on Earth and other planetary surfaces. We have identified structural patterns that we believe to be a consequence of lithospheric flexure due to volcanic loading and other features that may be associated with inflation of a magma reservoir beneath Tepev Mons. Concentric fractures surrounding Nyx Mons were mapped and their distributions examined. By modeling Nyx Mons as a surface load on an elastic plate, we used the concentric graben to provide a constraint on the effective elastic thickness at the time the volcano was emplaced. Our analysis indicates that, for an assumed Young's modulus for the plate of 10^{11} Pa and a load diameter of approximately 350 km, a lithospheric thickness of 50 km best describes the conditions at Nyx Mons at the time the concentric graben were formed. This predicted elastic thickness is in good agreement with Magellan gravity analyses. *Smrekar* [1994] indicates that the effective elastic thickness at short wavelengths is 30 $\pm$ 5 km, and 50 $\pm$ 5 at long wavelengths, where the 30 km value reflects a thinned elastic plate at the time the volcanoes were emplaced and the 50 km value represents present day elastic thicknesses. It should be noted that Smrekar was analyzing the overall highland swell, whereas this analysis models the individual volcanic loads in the region.

A concentric zone of weakness, represented by graben and coalesced chains of pit craters, surrounding Tepev Mons was also examined. These features, previously identified as possibly due to lithospheric flexure [*Solomon et al.*, 1992], occur on the steep flanks of the volcano. Our analysis indicates that they most likely formed as a result of extensional stresses associated with inflation and doming during magma chamber

inflation. Reservoir-induced stresses were analyzed using a finite element model, and our results indicate that inflation of a large sheet-like magma reservoir, represented by a horizontal ellipsoid in our model, most likely generated the zone of extension and fractures observed in Magellan images.

The tectonic deformation within the venusian edifices examined above can be compared and contrasted with two volcanic regions on Earth: Hawaii and the Galapagos Islands. These two volcanic areas differ markedly in their patterns of surface deformation. Kilauea volcano, located at the southeastern end of the Hawaiian island chain, exhibits two large rift zones extending east and southwest from the summit. Rift zones, linear patterns of extension on the scale of the individual edifices, form perpendicular to the direction of least compressive stress. The south flank of Kilauea is driven seaward over the downwardly flexed oceanic crust due to gravitational stresses inherent in its shape and by intrusions of high density magma along the rift zones. Stress accumulates due to repeated intrusions along the east rift zone, producing a net horizontal force within Kilauea's south flank. Opposed by only water on its seaward side, seismic and aseismic slip occurs at the interface between the volcanic pile and sedimented old ocean crust (a zone of weakness). The northern flank of Kilauea is buttressed by Mauna Loa, which prevents northward displacement of the edifice during dike intrusions [*Thurber*, 1988; *Dieterich*, 1988; *Ryan*, 1988].

In contrast to the Hawaiian volcanoes, the western Galapagos shield volcanoes lack prominent rift zones. The Galapagos islands are dominated by six large basaltic shield volcanoes believed to have formed over a hot spot now under Fernandina and Isabela islands. Galapagos shield volcanoes have steep slopes (15°-35°), broad flat summits and deep calderas which contribute to a distinct morphology relative to other shield volcanoes (e.g., Hawaii). The morphology of these shields results from surface processes such as gravitational relaxation, the emplacement of lava flow fields, and response to magma chamber stresses [*Cullen et al.*, 1987]. *Cullen et al.* [1987] suggested that the stress regime of the Galapagos shields hinders lateral drainage of magma and allows large volumes of melt to solidify as intrusions. Most of the eruptions on the Galapagos volcanoes are from linear or arcuate fissures (circumferential fissures around summit calderas, radial fissures lower on flanks) which *Chadwick and Howard* [1991] interpret to reflect patterns of underlying dikes from a subsurface magma chamber. The circumferential and radial diking has been attributed to episodes of broad volcano inflation and subsidence [*Chadwick and Howard*, 1991; *Simkin*, 1972] where dikes are emplaced perpendicular to the least compressive stresses.

Tepev Mons appears morphologically similar to the Galapagos volcanoes (steep flanks, broad summits, large calderas, and lack of rift zone deformation). Based on these discussions, the Galapagos islands may be the better terrestrial analog to Tepev Mons than typical Hawaiian volcanoes. As discussed above, there are no large regions of thru-going extension or rifting at Bell Regio, nor is there any indication of the more localized rifting that is evident on Kilauea. Recent work by *McGovern* [1996] indicates that the lack of these structures, important to the development of volcanoes on Earth and Mars, might result from an absence of a distinct layer of clay sediment, preventing the formation of the basal detachment beneath volcanoes such as those of the Galapagos chain.

The major edifices within Bell Regio may have been dominated by two distinct volcanic regimes. Lithospheric flexure appears to have occurred at both Tepev Mons (evident from the topographic moat) and Nyx Mons (resulting in the concentric graben). However, Tepev Mons appears to have experienced additional deformation due to the stresses associated with magma chamber inflation. Whereas the Tepev Mons load is relatively concentrated in a central region with a zone of fracturing surrounding the edifice and flows which are relatively limited in extent, Nyx Mons is much broader, with relatively expansive flows and large radial chains of pit craters possibly indicating a more distributed magmatic system. In the analysis by *McGovern and Solomon* [1995], a thick lithosphere is proposed as a precursor to the growth of a large shield volcano on Venus. A thin lithosphere would lead to plains-forming volcanism, or smaller shields. In our scenario, Nyx Mons, which is stratigraphically older, could represent the transitional state between broad, effusive plains volcanism to more shield-forming eruptions represented by Tepev Mons.

In addition, horizontal compressive stresses would increase as the edifice grows, inhibiting the easy rise to the surface and release of magma [*McGovern and Solomon*, 1995]. Therefore, for volcanism to occur in a construct as large as Tepev Mons, a pressurized magma reservoir, which we have postulated is responsible for this volcano's concentric fractures, would be needed. This pattern of increasing shield height and steeper flank slopes with decreasing apparent age is also supported by the presence of two very steep volcanoes on the SE flank of Tepev Mons. The flows from these steep edifices post-date those of Tepev and Nyx Montes, and are the likely source of the rough lava flow which traces the flexural moat north of Tepev Mons (Figure 1) [*Campbell and Rogers*, 1994]. The trends in surface deformation and volcano morphometry observed within Bell Regio may thus offer a view of the long-term history of a Venus highland rise, from early flood eruptions to late-stage centralized shield or dome-forming volcanism.

Acknowledgments. We gratefully acknowledge J. Melosh for providing the TECTON Code, B. Campbell for insightful discussions and software support, and P. McGovern and S. Smrekar for extremely helpful reviews. This work was supported in part by the NASA Planetary Geology and Geophysics Program.

References

Anderson, E. M., The dynamics of the formation of cone-sheets, ring dykes, and cauldron subsidence, *Proc. R. Soc. Edinburgh*, *56*, 128-157, 1935.

Anderson, E. M., *The Dynamics of Faulting*, 206 pp., Oliver and Boyd, London, 1951.

Artyushkov, E. V., Stresses in the lithosphere caused by crustal thickness inhomogeneities, *J. Geophys. Res.*, *78*, 7675-7708, 1973.

Banerdt, W. B., Global dynamic stress modeling on Venus, *Lunar Planet. Sci. XIX*, 25-26, 1988.

Bindschadler, D. L., and J. W. Head, Tessera terrain, Venus: Characterization and models for origin and evolution, *J. Geophys. Res.*, *96*, 5889-5907, 1991.

Borgia, A., J. Burr, W. Montero, L. D. Morales and G. E. Alvarado, Fault propagation folds induced by gravitational failure and slumping of the Central Costa Rica volcanic range: Implications for large terrestrial and Martian volcanic edifices, *J. Geophys. Res.*, *95*, 14357-14382, 1990.

Brace, W. F., and D. L. Kohlstedt, Limits on lithospheric stress imposed by laboratory experiments, *J. Geophys. Res.*, *85*, 6248-6252, 1980.

Campbell, B. A., and P. G. Rogers, Bell Regio, Venus: Integration of remote sensing data and terrestrial analogs for geologic analysis, *J. Geophys. Res.*, *99*, 21,153-21,171, 1994.

Chadwick, W. W. and K. A. Howard, The pattern of circumferential and radial eruptive fissures on the volcanoes of Fernandino and Isabela Islands, Galapagos, *Bull. Volcanol.*, *53*, 259-275, 1991.

Chevallier, L., and W. J. Verwoerd, A numerical model for the me-

chanical behavior of intraplate volcanoes, *J. Geophys. Res., 93*, 4182-4198, 1988.

Comer, R. P., S. C. Solomon, and J. W. Head, Elastic lithosphere thickness on the moon from mare tectonic features: A formal inversion, *Proc. Lunar Planet. Sci. Conf. 10th*, 2441-2463, 1979.

Comer, R. P., S. C. Solomon, and J. W. Head, Mars: Thickness of the lithosphere from the tectonic response to volcanic loads, *Rev. Geophys., 23*, 61-92, 1985.

Cullen, A. B., A. R. McBirney, and R. D. Rogers, Structural controls on the morphology of Galapagos shields, *J. Volcanol. Geotherm. Res., 34*, 143-151, 1987.

Davis, P. M., Surface deformation due to inflation of an arbitrarily oriented triaxial ellipsoidal cavity in an elastic half space, with reference to Kilauea volcano, Hawaii, *J. Geophys. Res., 91*, 7429 - 7438, 1986.

Dieterich, J. H., Growth and persistence of Hawaiian volcanic rift zones, *J. Geophys. Res., 93*, 4258-4270, 1988.

Dieterich, J. H., and R. W. Decker, Finite element modeling of surface deformation associated with volcanism, *J. Geophys. Res., 80*, 4094-4102, 1975.

Filson, J., T. Simkin, and L. Leu, Seismicity of a caldera collapse: Galapagos Islands 1968, *J. Geophys. Res., 78*, 8591-8622, 1973.

Fleitout, L., and C. Froidevaux, Tectonics and topography for a lithosphere containing density heterogeneities, *Tectonics, 1*, 21-56, 1982.

Fleitout, L., and C. Froidevaux, Tectonic stresses in the lithosphere, *Tectonics, 2*, 315-324, 1983.

Forsyth, D. W., Subsurface loading and estimates of the flexural rigidity of continental lithosphere, *J. Geophys. Res., 90*, 12,623-12,632, 1985.

Golombek, M. P., Fault type predictions from stress distributions on planetary surfaces: Importance of fault initiation depth, *J. Geophys. Res., 90*, 3065-3074, 1985.

Hall, J. L., S. C. Solomon, and J. W. Head, Elysium region, Mars: Tests of lithospheric loading models for the formation of tectonic features, *J. Geophys. Res., 91*, 11,377-11,392, 1986.

Head, J. W., and L. Wilson, Magma reservoirs and neutral buoyancy zones on Venus: Implications for the formation and evolution of volcanic landforms, *J. Geophys. Res., 97*, 3877-3903, 1992.

Jaeger, J. C., and N. G. W. Cook, Fundamentals of rock mechanics, 593 pp., Chapman and Hall, London, 1979.

Janes, D. M., Tectonics of planetary loading: A general model and results, *J. Geophys. Res., 95*, 21,345-21,355, 1990.

Janle, P., D. Jannsen, and A.T. Basilevsky, Tepev Mons on Venus: Morphology and elastic bending models, *Earth Moon Planets, 41*, 127-139, 1988.

Marsh, B. D., On the mechanics of caldera resurgence, *J. Geophys. Res., 89*, 8245-8251, 1984.

McGovern, P.J., *Studies Of Large Volcanoes on the Terrestrial Planets: Implications For Stress State, Tectonics, Structural Evolution, And Moat Filling*, Ph.D. thesis, 339 pp., Mass. Inst. of Technol., Cambridge, 1996.

McGovern, P. J., and S. C. Solomon, Estimates of elastic plate thicknesses beneath large Volcanoes on Venus, International Colloquium on Venus, *LPI Contrib., 789*, 68-70, 1992.

McGovern, P. J., and S. C. Solomon, State of stress, faulting, and eruption characteristics of large volcanoes on Mars, *J. Geophys. Res., 98*, 23,553-23,579, 1993.

McGovern, P. J., and S. C. Solomon, Factors affecting the growth, development, and structure of large volcanoes on Venus, *Lunar Planet. Sci. XXVI*, 939-940, 1995.

McGovern, P. J., and S. C. Solomon, Filling of flexural moats around large volcanoes on Venus: Implications for volcano structure and global magmatic flux, *J. Geophys. Res., 102*, 16,303-16,318, 1997.

McKenzie, D., and J. Jackson, The relationship between strain rates, crustal thickening, palaeomagnetism, finite strain and fault movements within a deforming zone, *Earth Planet. Sci. Lett., 65*, 182-202, 1983.

McNutt, M., Lithospheric stress and deformation, *Rev. Geophys., 25*, 1245-1253, 1987.

McNutt, M. and L. Shure, Estimating the compensation depth of the Hawaiian swell with linear filters., *J. Geophys. Res., 91*, 13,915-13,923, 1986.

McTigue, D. F., and C. C. Mei, Gravity-induced stresses near topography of small slope, *J. Geophys. Res., 86*, 9268-9278, 1981.

Melosh, H. J., On the origin of fractures radial to lunar basins, *Proc. Lunar Sci. Conf., 7th*, 2967-2982, 1976.

Melosh, H. J., The tectonics of mascon loading, *Proc. Lunar Planet. Sci. Conf. 9th*, 3513 - 3525, 1978.

Melosh, H. J., and A. Raefsky, A simple and efficient method for introducing faults into finite element computations, *Bull. Seismol. Soc. Am., 71*, 1391-1400, 1981.

Melosh, H. J., and C. A. Williams, Mechanics of graben formation in crustal rocks: A finite element analysis, *J. Geophys. Res., 94*, 13961-13973, 1989.

Mogi, K., Relations between the eruptions of various volcanoes and the deformation of the ground surfaces around them, *Bull. Earthquake Res. Inst., 36*, 99-134, 1958.

Nakamura, K., Volcanoes as possible indicators of tectonic stress orientation - Principle and proposal, *J. Volcanol. Geotherm.* Res., *2*, 1-16, 1977.

Pollard, D. D., and O. H. Muller, The effect of gradients in regional stress and magma pressure on the form of sheet intrusions in cross section, *J. Geophys. Res., 81*, 975-984, 1976.

Price, N. J., and J. W. Cosgrove, *Analysis of geological structures*, 502 pp., Cambridge Univ. Press, New York, 1990.

Richardson, R., C., Solomon and N. Sleep, Intraplate stress as an indicator of plate tectonic driving forces, *J. Geophys. Res., 81*, 1847-1856, 1976.

Rowland, S. K. and D. C. Munro, The caldera of Volcan Fernandina: A remote sensing study of its structure and recent activity, *Bull. Volcanol., 55*, 97-109, 1992.

Rundle, J. B., Deformation, gravity, and potential changes due to volcanic loading of the crust, *J. Geophys. Res., 87*, 10,729-10,744, 1982.

Rundle, J. B., and J. H. Whitcomb, A model for deformation in Long Valley, California, 1980-1983, *J. Geophys. Res., 89*, 9371-9380, 1984.

Ryan, M. P., The mechanics and three-dimensional internal structure of active magmatic systems: Kilauea volcano, Hawaii, *J. Geophys. Res., 93*, 4213-4248, 1988.

Schultz, R. A., and M. T. Zuber, Observations, models, and mechanisms of failure of surface rocks surrounding planetary surface loads, *J. Geophys. Res., 99*, 14,691-14,702, 1994.

Senske, D. A., G. G. Schaber, and E. R. Stofan, Regional topographic rises on Venus: Geology of Western Eistla Regio and comparison to Beta Regio and Atla Regio, *J. Geophys. Res., 97*, 13,395-13,420, 1992.

Smrekar, S. E., Evidence for active hotspots on Venus from analysis of Magellan gravity data, *Icarus, 112*, 2-26, 1994.

Solomon, S. C., J. W. Head, and R. P. Comer, Thickness of the martian lithosphere from tectonic features: Evidence for lithospheric thinning beneath volcanic provinces, *NASA TM 80339*, 60-62, 1979.

Solomon, S. C. and J. W. Head, Lithospheric flexure beneath the Freyja Montes foredeep, Venus: Constraints on lithospheric thermal gradient and heat flow, *Geophys. Res. Lett.*, 17, 1393-1396, 1990.

Solomon, S. C., S. E. Smrekar, D. L. Bindschadler, R. E. Grimm, W. M. Kaula, G. E. McGill, R. J. Phillips, R. S. Saunders, G. Schubert, S. W. Squyres, and E. R. Stofan, Venus tectonics: An overview of Magellan observations, *J. Geophys. Res., 97*, 13,199-13,255, 1992.

Thomas, P. J., S. W. Squyres, and M. H. Carr, Flank tectonics of Martian volcanoes, *J. Geophys. Res., 95*, 14345-14355, 1990.

Thurber, C. H., Flexure and seismicity beneath the south flank of Kilauea volcano and tectonic implications, *J. Geophys. Res., 93*, 4271-4278, 1988.

Walker, G. P., Downsag calderas, ring faults, caldera sizes, and incremental caldera growth, *J. Geophys. Res., 89*, 8407-8416, 1984.

Walsh, J. B., and R. W. Decker, Surface deformation associated with volcanism, *J. Geophys. Res., 76*, 3291-3302, 1971.

Williams, K. K., and M. T. Zuber, An experimental study of incremental surface loading of an elastic plate: Application to volcano tectonics, *Geophys. Res. Lett., 22*, 1981-1984, 1995.

Zuber, M. T., and P. J. Mouginis-Mark, Caldera subsidence and magma chamber depth of the Olympus Mons Volcano, Mars, *J. Geophys. Res., 97*, 18,295-18,307, 1992.

P.G. Rogers, MRC 315, Smithsonian Institution, Washington, DC 20560. (e-mail: rogers@ceps.nasm.edu)

M.T. Zuber, Department of Earth, Atmospheric, and Planetary Sciences, Massachusetts Institute of Technology, Cambridge, MA 02139. (e-mail: zuber@tharsis.gsfc.nasa.gov)

(Received September 24, 1996; revised February 17, 1998; accepted February 19, 1998.)